Available online at www.sciencedirect.com
ScienceDirect
International Journal of Pharmaceutics 351 (2008) 236–243
INTERNATIONAL JOURNAL OF PHARMACEUTICS
www.elsevier.com/locate/ijpharm

Understanding a relaxation behavior in a nanoparticle suspension for drug delivery applications

Z. Deng [a,*], S. Xu [b], S. Li [b]

[a] Department of Analytical Development, 1010 Joaquin Road, M4-2A, ALZA Corp., Mountain View, CA 94043, USA
[b] Department of Pharmaceutical Development, 1010 Joaquin Road, M4-2B, ALZA Corp., Mountain View, CA 94043, USA

Received 7 July 2007; received in revised form 28 September 2007; accepted 2 October 2007
Available online 10 October 2007

Abstract

Nanoparticle dispersion has demonstrated its effectiveness in improving the dissolution rate and oral bioavailability of poorly water-soluble compounds. When we studied the interactions of drug and polymeric stabilizers and milling parameters of a poorly water-soluble compound, Compound A, the relaxation behavior that occurred repeatedly in our nanoparticle dispersion formulation was observed. Nanomill® was used to generate the nanoparticle dispersion, and milling parameters such as time, speed, and stabilizer loading were altered to investigate their effects on relaxation. The particle size and morphology of milled products were studied using a light-scattering particle analyzer and a scanning electron microscope (SEM). X-ray powder diffraction (XRD) was employed to characterize particle crystallinity and the crystallite size. The results indicated that, after milling, nanoparticles agglomerated constantly to form clusters and reached maximum apparent size within the first 24 h. Thereafter, the clusters relaxed spontaneously and, within a few days, dissociated into individual primary particles and the suspension were stable at sub 100-nm levels near equilibrium. Milling crystalline drug substance resulted in an XRD pattern in which the peaks were observed to broaden, suggesting formation of disordered nanocrystalline. Altering milling conditions and stabilizer ratios influences the relaxation behavior and certainly led to optimization of the process and performance of nanoparticle suspension formulations.

Keywords: Poorly water-soluble compounds; Nanoparticle; Drug delivery; X-ray powder diffraction (XRD) and Scanning electron microscope (SEM)

1. Introduction

Many of the new chemical entities are considered Biopharmaceutic Class II-low solubility and high permeability, according to the Biopharmaceutics Classification System (BCS) (FDA, 2000). A major challenge in developing poorly water-soluble drug candidates is dissolution-rate-limited bioavailability. When evaluating the performance of molecules formulated using conventional methods, the performance of drug in preclinical screens is often highly variable. The dissolution rate of a drug is a function of its intrinsic solubility and particle size. As described by the Nernst–Brunner and Levich modification of the Noyces–Whitney model of dissolution, the surface area of poorly water-soluble drug is directly proportional to its rate of dissolution (Dressman et al., 1998). A new drug delivery approach for poorly water-soluble drug is reduction of the compound's particle size into nanometer-sized drug crystals to enhance dissolution (Kawashima, 2001). There are various approaches for production of nanoparticle drug formulations. The methods include wet milling (Merisko-Liversidge et al., 1996), high-pressure homogenization (Wissing and Muller, 2001) and supercritical fluid extraction emulsion (Shekunov et al., 2005) One novel particle engineering technology is based on NanoCrystal® technology (Elan Drug Delivery, King of Prussia, PA, USA), in which poorly water-soluble drugs are formulated as nanoparticle drug crystal using high-shear mills (Liversidge et al., 1991) Nanocrystalline dispersions are prepared using a media milling process (Merisko-Liversidge et al., 2003). The milling chamber is charged with milling media, water, drug, and stabilizers. The shear force, generated during impact of the milling media and the drug, provides the energy input to fracture drug crystals into nanoparticles. The challenge of particle-size control in nanoparticle dispersion is that most small-molecule drugs tend to form relatively large

* Corresponding author. Tel.: +1 650 564 2571; fax: +1 650 564 4212.
E-mail address: rdeng@alzus.jnj.com (Z. Deng).

0378-5173/$ – see front matter © 2007 Elsevier B.V. All rights reserved.
doi:10.1016/j.ijpharm.2007.10.001

crystals in the 10–100-μm size range. To stabilize nanoparticle dispersion and inhibit the crystal growth, triblock polymer (F108), polyvinyl pyrrolidone (PVP K30), copolymer Plasdone S630, and substituted cellulosic polymer (HPC, HPMC) are usually required as GRAS (generally recognized as safe) stabilizers in NanoCrystal® technology. These stabilizers are used to wet constituent particles by eliminating air and also provide particle steric and static stabilization. In addition, they reduce solid surface energy by adsorption and decrease viscosity by preventing flocculation and creeping of stabilizer molecules along grain boundaries or in dislocations that occur under shear stress (Rebinder effect). Inadequate stabilizer in nanoparticle dispersions induces agglomeration or aggregation, while an excess promotes Ostwald ripening (larger crystals growing at expense of smaller crystals). To inhibit the latter and prevent recrystallization, flocculation, and phase separation, ideal nano formulation design takes advantage of synergistic interactions between certain polymers and ionic surfactants.

We evaluated a nanoparticle dispersion formulation to enhance the dissolution of the poorly water-soluble compound, Compound A (Johnson & Johnson Pharmaceutical Research & Development, L.L.C., Raritan, NJ, USA). The post-milling relaxation in the nanoparticle suspension must be controlled and minimized because an unpredictable size-evolution profile is undesirable for subsequent processes, such as spray drying or lyophilization. Relaxation occurred in the drug suspension refers to an abnormal behavior that drug formulation system is most likely to be driven far from thermodynamic equilibrium under high shear milling. The system that is far from equilibrium state became unstable and evolves to a new organized state. This relaxation behavior can be briefly described as follows: upon stopping milling, the apparent particle size and viscosity continuously increase. In one day or so, apparent particle size reaches a maximum and the system turns into immovable gel. Thereafter, gel 'melt' and suspension turns into free flow state in few days. The particle size continuously decreases up to 82 nm. The size continually shows excellent long-term shelf stability. The purpose of this study was to investigate the relaxation profile of the Compound A nanoparticle dispersion. Compound A was processed using various milling conditions and different formulations. The relaxation of nanoparticle dispersion was characterized using particle size analysis, X-ray diffraction (XRD), and scanning electron microscopy (SEM). Controlling the post-milling relaxation in the nanoparticle dispersion was critical to produce stable nanoparticle dispersions in order to enhance dissolution properties of Compound A, which is poorly water-soluble. At this writing, we found no other reports describing relaxation phenomena in nanoparticle drug dispersions.

2. Materials and methods

2.1. Materials

Compound A was the poorly water-soluble model drug investigated. Plasdone S-630 (Copoviodone, Vinyl pyrrolidone/vinyl acetate copolymer, CAS No 25086-89-9,ISP Technologies Inc,

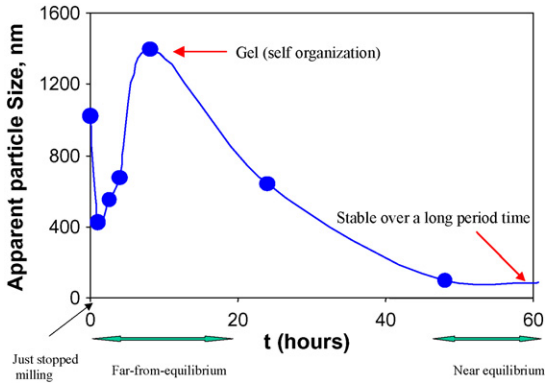

Fig. 1. Nanoparticle dispersion relaxation phenomenon.

Wayne, NJ, USA) and Docusate Sodium, USP (Cytec Industries Inc, West Paterson, NJ, USA) were used to stabilize the Compound A nanoparticle dispersion. A 0.5-mm cross-linked polystyrene milling media (PolyMill-500 USP, Elan Drug Delivery, King of Prussia, PA, USA) was used in the milling process.

2.2. Preparation of nanoparticle suspension and lyophilization of suspension

The nanoparticle drug suspensions were milled in 50-mL batches using a NanoMill-01 Systems milling apparatus manufactured by Elan Drug Delivery (King of Prussia, PA, USA). The drug slurry was prepared by mixing compound A with the solution containing 4.10% Plasdone S-630 (ISP, Inc., Wayne, NJ, USA) and 0.295% Docusate Sodium, USP (Cytec Industries Inc., West Paterson, NJ, USA). The slurry was loaded into in the 50-mL milling chamber. PolyMill-500 USP (0.5 mm) milling beads (Elan Drug Delivery, King of Prussia, PA, USA) w loaded into chamber and gently mixed with the drug slurry. The recycle chiller temperature was set at 5 °C. The mill was running for ~1 min at 1800 rpm before the milling speed was gradually increased to 4400 rpm. The drug dispersion was harvested after milling for 40–60 min, with an ~85% yield. The apparent particle size changed with time, increasing initially and might gel,

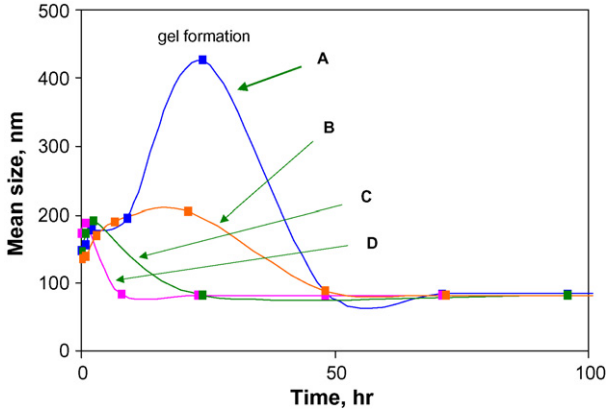

Fig. 2. Effects of milling conditions and formulation compositions on relaxation. (A) Original formulation (high-shear rate); (B) extended milling time; (C) increased surfactant; (D) diluted surfactant solution post milling (all curves here represent milling at 4.4k rpm).

Table 1
Formulation of nanoparticle dispersion, milling process parameters and mean particle size

Experiment code	Formulation drug%/S630%/DS%	Milling speed (rpm)	Milling time (min)	Particle size (nm) (after relaxation)
A	15/3.5/0.25	4400	40	82
B	15/3.5/0.25	4400	60	82
C	15/3.5/0.50	4400	40	82
D	15/3.5/0.25	4400	40	82
E	15/3.5/0.25	2930	60	86

then decreasing to 82 nm in a few days after milling as shown in Figs. 1 and 2. To investigate this distinct relaxation phenomenon, a series of batches of nanoparticle suspension were prepared as described in Table 1. The suspension was freeze-dried under vacuum for 3 days in the Labconco Freezone 6 Liter Benchtop Freeze Dry System (Labconco Corporation, Kansas City, Missouri, USA). The compositions of the final dried formulation was given as 56% API 934, 40.6% Plasdone S630 (ISP), 3.4% DOSS. The lyophilized powder was stored in a glass jar with plastic lid in a desiccator at room temperature.

2.3. Canine bioavailability

An amount of powder formulation containing 25 mg drug was weighed into a size 0 HPMC V-cap (Capsugel, Greenwood, SC) for dosing. The dose per capsule was verified by HPLC analysis. The capsules were orally dosed followed with water to non-naïve male beagle dogs weighing 11–14 kg. No IV dosing for absolute bioavailability determination was conducted. There was at least a 2 week wash-out period between dosing. The dogs were fasted for 15–18 h pre-dose and 6–7 h post-dose. Blood (~2 mL/timepoint) was collected from the cephalic and saphenous veins and/or the jugular arteries at $t = 0$ (pre-dose) and $t = 0.5$, 1, 2, 4, 6, 9, and 12 h post-dose. Sodium heparin was used as the anticoagulant. Plasma samples were prepared by centrifugation at 2500 rpm at 4 °C for 10 min and stored at −20 °C until analysis.

Fifty microliters of the plasma sample was mixed with 300 μL of acetonitrile containing 50 ng/mL of the internal standard. The samples were filtered and 10 μL was injected into an Applied Biosystems (Foster City, CA, USA) API 3000 LC/MS/MS system. Separation was achieved with a MetaChem Polaris, 3 μ C18-A 100 mm × 3.0 mm column (Varian, Palo Alto, CA, USA) at room temperature with a flow rate of 0.42 mL/min. The mobile phase was A: 10 mM ammonium acetate in d.i. water and B: 100% acetonitrile. Elution was achieved with a linear gradient from 60 to 95% B from 0.1 to 0.5 min, constant 95% B from 0.5 to 2.5 min, and then a linear gradient from 95 to 60% from 2.5 to 3.0 min. Total run time was 4 min. For mass spectrometry, a turbo spray ion source with a 5500 V ion spray voltage and 550 °C temperature was used. The compound was detected by multiple reaction mode scanning. A calibration curve from 1 to 1000 ng/mL was constructed from seven standard concentrations. Quantification of Compound A was based on weighted linear regression analysis of the standard peak areas, with a limit of quantification of 1 ng/mL.

The area under the curve for 0–12 h ($AUC_{(0–12\,h)}$) was calculated from the plasma concentration vs. time data using the linear trapezoid method. Pair-wise comparisons of the $AUC_{(0–12\,h)}$ and $Cmax_{(0–12\,h)}$ values for the different formulations were performed using a two-sided, equal variance *t*-test. Depending on the study design, either paired or non-paired *t*-tests were performed as appropriate.

2.4. Particle size analysis (PSA)

The particle size of each nanoparticle suspension was monitored by using a Horiba LA-910 laser scattering particle size distribution analyzer (Model LA-910, HORIBA, Ltd. Kyoto, Japan) to assess suspension quality. A high-quality suspension exhibits remarkable stability in particle size with minimal aggregation and crystal growth from ripening processes. Each formulation sample was stored at room temperature in the laboratory. Prior to sizing suspension, samples were diluted with freshly filtered de-ionized water. Periodically, a small quantity of each formulation was dispersed into the circulation reservoir of a Horiba LA-910 till the blue light intensity dropped in the range of 80 ± 1%. The particle-size-distribution analyzer uses uni-modal analysis of intensity distribution for mean particle size determination. Mean particle size was measured without sonication and with 30 s of sonication to determine if agglomeration was an issue.

2.5. Scanning electron microscopy (SEM)

An FEI Quanta 200 FEG field emission environmental scanning electron microscope (FEI Co., Hillsboro, Oregon, USA) operating at 5 keV, a spot-size setting of 1.0, and a working distance of 5 mm, was used to obtain SEM photomicrographs of the various samples in the high-vacuum mode. Prior to SEM analysis, samples were diluted and an aliquot of the diluted preparation was dispersed on OEM GE PCTE (Polycarbonate) 0.05-μm filter membranes (GE Osmonics Labstore, Minnetonka, USA) placed on a carbon-tape-coated aluminum stub. Samples were dried and then coated with 5 nm of platinum–palladium mixture using a 208HR high-resolution sputter coater (Cressington Scientific Instruments Ltd., Watford, UK).

2.6. X-ray diffraction (XRD)

A PANalytical X'Pert PRO PW3040-Pro X-ray diffractometer (PANalytical, Almelo, The Netherlands) equipped with an

X'celerator™ detector was used to obtain X-ray diffraction patterns. With the X-ray generator set at 45 kV and 40 mA, a copper anode was used to produce a divergent beam with an average Kα wavelength of 1.541874 Å. The range of 4–45° 2θ with a step size of 0.0170° 2θ and a count time of 29.84 s per step were used for the measurements. The room-temperature measurements were conducted on a spinner stage operating at a rotational speed of one revolution per two seconds. X'Pert Highscore™ data analysis software version 1.0 d (PANalytical, Almelo, The Netherlands) was used to find peak parameters.

The nanoparticle suspension was transferred via pipette to the center of a silicon zero-background sample plate (10-mm diameter, 1-mm cavity; The Gem Dugout, State College, PA 16803 USA). Using a programmable divergence slit and a programmable receiving slit, a spot of 11.5 mm from about the center of the plate was irradiated with the source; the detector observed the central 10 mm of the sample plate. The dried nanoparticles were measured with and without a gentle mortar/pestle grounding.

In X'Pert HighScore analysis, the SCHERRER calculator (Scherrer, 1918) determines crystallite size by comparing the profile width of a standard profile with a sample profile according to the SCHERRER formula or according to the tangent formula. The basis of the simple size-strain analysis is the following formula:

The SCHERRER formula:

$$\text{Crystallite size (average)} = \frac{K\lambda}{(B\cos\theta)}$$

B describes the structural broadening, which is the difference in integral profile width between a standard and the unknown sample.

The crystallinity is calculated by separating intensities due to amorphous and crystalline phase on diffraction phase (Chung, 1974). A computer-aided, curve-resolving technique is used to separate crystalline and amorphous phases of diffracted graph. Using X'Pert HighScore, the normalization assumes that the sum of all identified phases is 100%. This means there are no unidentified crystalline phases, nor any amorphous phases present in the sample. Only under these conditions can meaningful semi-quantitative results be obtained.

After separation, the total area of the diffracted pattern is divided into crystalline (A_C) and amorphous components (A_a).

Percentage of crystallinity X_C% is measured as ratio of crystalline area to total area.

$$X_{C\%} = \left\{ \frac{A_c}{A_a} + A_c \right\} \times 100(\%) \quad (5)$$

where A_C = area of crystalline phase, A_a = area of amorphous phase, X_C = percentage of crystallinity.

3. Results

3.1. Particle size analysis

The suspension stability was monitored using PSA and SEM. The PSA profile of the apparent particle size as a function of suspension holding time after milling is shown in Fig. 1 upon stopping milling, the mean (apparent) particle size of the nanoparticle suspension was ~400 nm. Nanoparticle suspensions were prepared routinely with mean particle sizes that averaged 80 nm for Compound A formulation (Table 1). The apparent particle size increased within the first 24 h after the milling was stopped. In fact, the individual particle size did not grow up. The apparent particle size increase was coming from particles agglomeration and self-organization. Gel formation was observed for the nanoparticle suspension holding on the shelf for ~1 day after high shear milling. Generally, the apparent particle size reached the maximum within 14–48 h after milling stopped, depending on milling parameters and formulation composition (Fig. 2). During storage, the samples were left alone without agitation, shaking or any disturbance. After reaching the peak mean size range the gel started 'melt' and the apparent particle size of the suspension constantly decreased. Depending on the milling conditions and formulation composition, the profile of the apparent particle size as a function of dispersion holding time was variable. Our results suggest that relaxation of the particles could be alleviated by increasing surfactant loading, increasing shear rate, or extending the milling time as shown in Fig. 2.

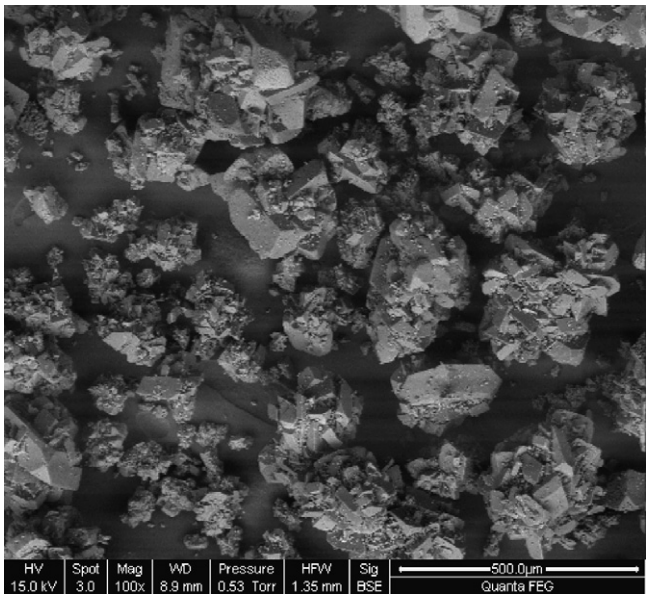

Fig. 3. SEM micrographs of the raw drug.

3.2. Scanning electron microscopy

SEM micrographs of the various samples containing Compound A are shown in Figs. 3 and 4. Fig. 3 shows the surface morphology of raw Compound A. The bulk Compound A crystals had particle sizes 100–300 μm in length and were rectangular and aggregated. In Fig. 4a, the scanning electron micrographs show representative images of the nanoparticle drug suspension within 1 h after stopped milling. It is evident that the morphology of milled drug nanoparticles was significantly different from that of the rectangular-shaped raw drug

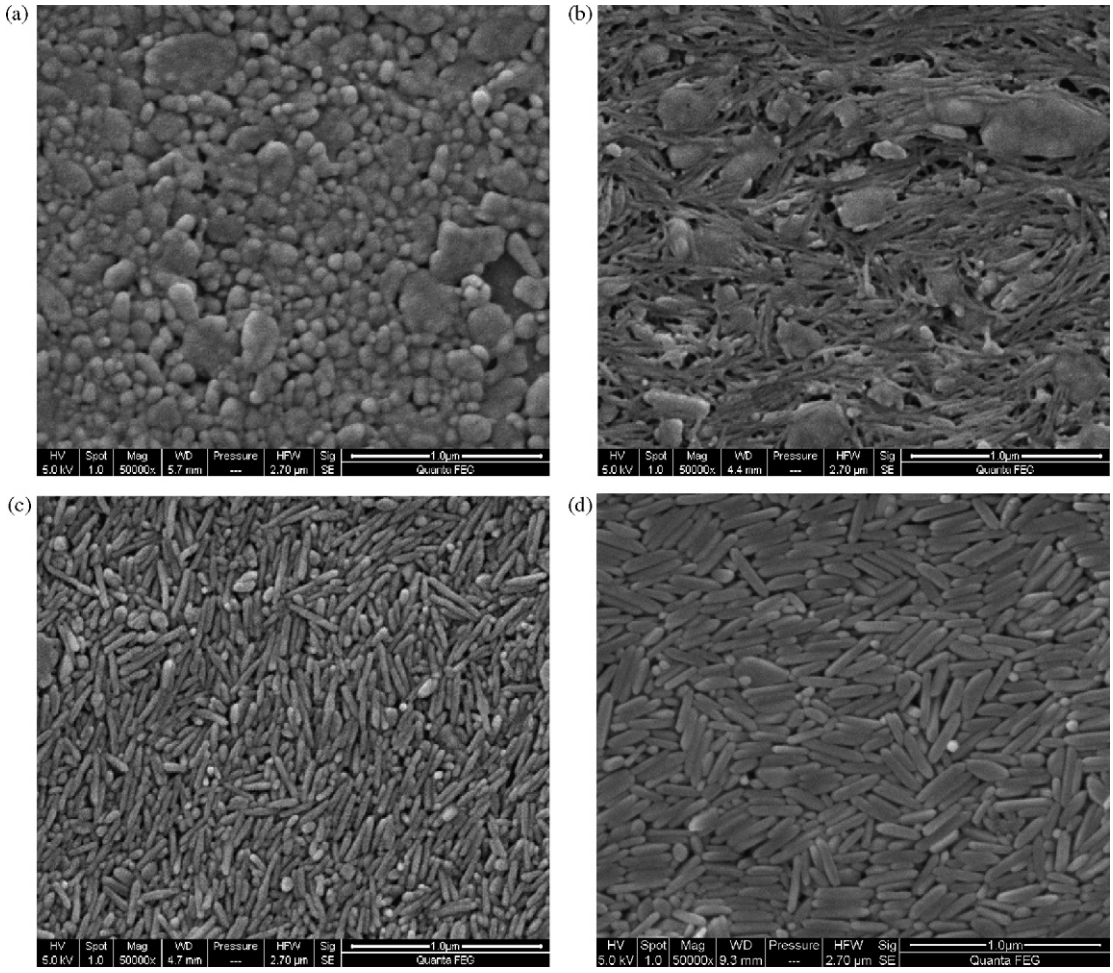

Fig. 4. SEM micrographs of nanosized drug particles as a function of sample holding time: (a) $t = 0$ Fresh milled; (b) $t = 24$ h; (c) $t = 6$ days; (d) $t = 2$ years.

crystals. As expected, nanoparticle agglomeration following milling is clearly observed in SEM micrographs. These micrographs show Compound A formed circular-, and rod-shaped nanoparticles with a mean particle size of 80–100 nm. Upon closer investigation, a portion of the milled nanoparticles can be seen as aggregates and agglomerates of several smaller particles that are not as uniformly sized and shaped. It seems that the nanoparticle suspension aggregated, agglomerated, and remained physically unstable after milling. Following 24 h at room temperature, a gel is formed. Fig. 4b shows the surface morphology of nanoparticles from the gelled nanoparticle dispersion. The surface morphology of nanoparticles resembles an elongated needle-like structure that is significantly larger than the fresh milled nanoparticles. The needle-like structures appear to blend with the circular-shaped nanoparticle aggregates and agglomerates originally observed. In the high-magnification SEM micrograph, the needle-like structures are more distinct. The needle-like structures consist of the globular-shaped nanoparticles that aggregate and agglomerate into a linear structure. After 6 days storage at room temperature without any agitation, the gel formation and the needle-like structures dissociated; Fig. 4c shows most nanoparticles were rod-shape and globular-shaped. The aggregate and agglomerate originally observed on fresh-milled nanosuspension are absent, and the nanoparticles are more distinguishable and uniform in size. After 2 years at room temperature, the mean particle size of nanoparticle was 85 nm, relatively unchanged from 82 nm in a 6-day measurement. Upon close investigation by SEM, most of the globular-shaped nanoparticles became rod-shaped (Fig. 4d.). These nanoparticles are larger and more uniform compared with the 6-day sample (Fig. 4c). The boundaries between the nanosized globular-shaped and rod-shape particles are less apparent, with the globular nanoparticles "melting" into rod shapes after long storage. The rod-shape of nanoparticles may be dictated by the morphology of unprocessed crystalline powder and the fracture plane of crystals and drug/stabilizer interactions. When optimally stabilized though, the nanoparticle dispersion did not aggregate or agglomerate, and remained stable for a least 2 weeks post milling. It is evident that freshly milled Compound A nanoparticles had a different surface morphology than the stabilized Compound A nanoparticles.

3.3. X-ray diffraction studies

The XRD pattern of raw un-milled Compound A is shown in Fig. 5. The bulk Compound A exhibited intense crystalline peaks between 10° and 30° 2θ. The XRD patterns of milled nanoparticle Compound A are shown in Fig. 6. The milled nanoparticle

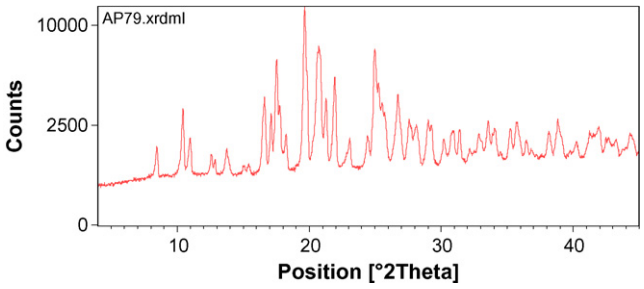

Fig. 5. XRD pattern of the raw drug.

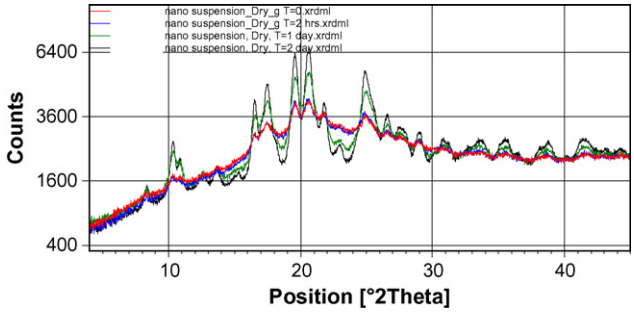

Fig. 6. XRD patterns of nanosized drug particles as a function of sample holding time: $t = 0$ (red), $t = 2$ h (blue), $t = 1$ day (green) and $t = 2$ days (black).

dispersion produced a broad halo as is characteristic of amorphous material, indicating the milled sample had a different crystalline structure than bulk Compound A. Crystalline peaks from Compound A were seen in XRD patterns at 16.6°, 17.5°, 19.6°, 20.7° and 21.9° 2θ. As seen in Fig. 6, the crystalline peak intensity was significantly decreased, indicating the high-shear milling process interfered with the crystalline state of bulk drug. The reduction in peak intensity and a broad halo characteristic may be due to particle size reduction and change of crystallinity of the active ingredient, rather than dilution of nanoparticle particles in Plasdone S-630 and docusate sodium, USP formulations. Nanoparticles showed further increases in peak intensity as a function of the duration of storage time at room temperature. Milling crystalline drug substance results in an XRD pattern in which the peaks are observed to broaden, suggesting formation of a disordered nanocrystalline structure. Such materials are solids that have lost their long-range crystalline order but are not amorphous. The broad amorphous halos observed in disordered nanocrystalline materials are related to the crystalline microstructure (crystal size, micro-strain and defects) and correlated with parent crystalline peaks. The calculated mean coherent crystal domain size for the nanoparticles just after milling was stopped was 13 nm (Table 1), indicating a disordered nanocrystalline was formed. The crystal size then increased from 13 to 23 nm over 6 days. Assuming that crystalline materials give rise to sharp peaks, and amorphous materials yield broad halo peaks, percent crystallinity is the normalization ratio between the integrated crystalline peaks and the amorphous "background". The percent of crystallinity increased rapidly and then stabilized ~2 days after milling (Table 2). There may be a continuum of state between long-range order and short-range order for disordered nanocrystalline, in which the short-range order increases to equal the long-range order with storage at room temperature. Alternatively, the result may be a function of an amorphous component as suggested by the halo shape seen in Fig. 6. Rietvelt

Table 2
Fit XRD peak profile and crystallite size calculation (sample at $t = 6$ day)

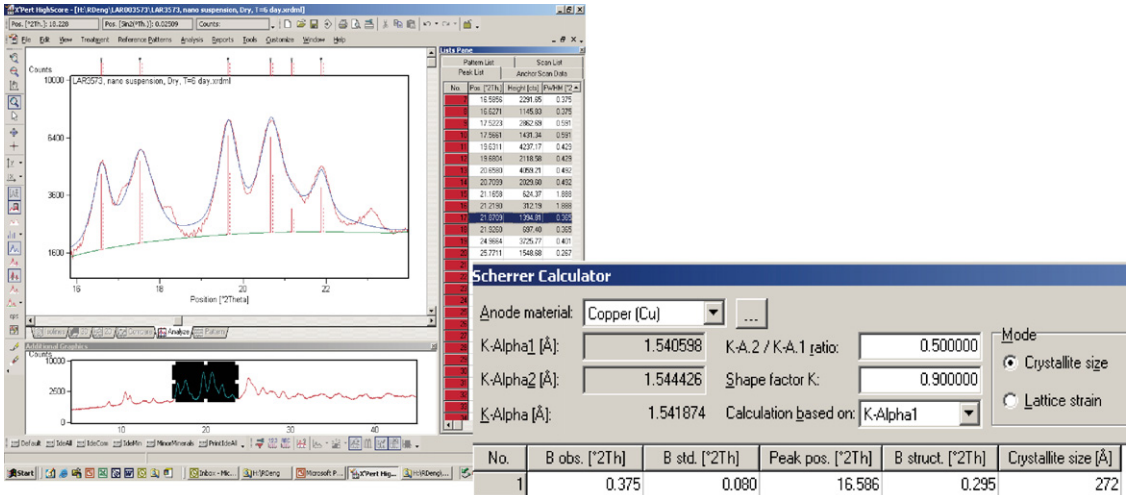

No.	B obs. [°2Th]	B std. [°2Th]	Peak pos. [°2Th]	B struct. [°2Th]	Crystallite size [Å]
1	0.375	0.080	16.586	0.295	272
2	0.591	0.080	17.522	0.511	157
3	0.429	0.080	19.631	0.349	231
4	0.492	0.080	20.658	0.412	196
5	0.365	0.080	21.871	0.285	284

Mean: 23 nm

X-ray diffraction only sees the crystallite size (or mean coherent domain size), not the particle size.

Mean: 23 nm. X-ray diffraction only sees the crystallite size (or mean coherent domain size), not the particle size.

Table 3
Calculated percent of crystallinity and calculated crystallite size

Nanoparticle from dispersion at different holding times	Calculated% crystallinity	Calculated mean coherence crystal domain size (nm)
0	7	13
2 h	8	14
1 day	19	15
2 day	29	21
3 day	30	21
6 day	31	23

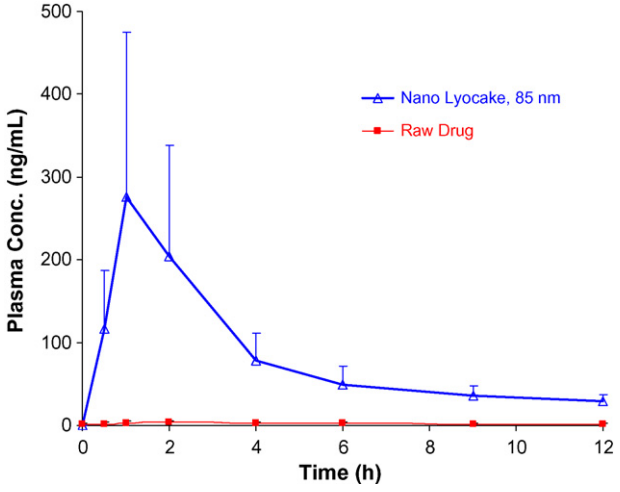

Fig. 7. Plasma concentration time curve of the raw drug and lyophilized nanoparticle dispersion solid formulation.

molding (Bates et al., 2006) for milled nanoparticles remains to be studied (Table 3).

3.4. Efficacy of nanoparticle drug suspension

To evaluate efficacy, the lyophilized nanoparticle drug dispersion were tested in dogs. Results of these studies are shown in Fig. 7. The graph shows the plasma concentration time curve of Compound A. The solid lyocake formulation (Drug%/S630%/DOOS%, 56/40.6/3.4) was administered orally at identical dose (25 mg) to fasted dogs as lyophilized nanoparticles or raw drug Compound A. In this study, the bioavailability of Compound A was significantly improved as the particle size of raw drug was reduced from 20 μm to 85 nm. This pattern of results is routinely observed in different nanoparticle dispersions and lyophilized or spray dried solid formulations when the primary factors affecting the bioavailability of the drug are rate and extent of dissolution.

4. Discussion

A poorly water-soluble compound, Compound A was formulated with polymer S630 and surfactant docusate sodium to form a stable nanoparticle suspension formulation using high-shear milling. The drug suspension displayed a distinct relaxation behavior when milling was stopped. Experiments were designed to identify the effect of the milling conditions and stabilizers loading on the relaxation profile. Light-scattering size, SEM, and XRD were employed to monitor the progress of particle size and morphology during relaxation course. The SEM observation clearly indicated that after milling, globular primary nanoparticles agglomerated to form bar clusters that elongated continuously to from needle-like clusters, which tends to bundle together within the first 24 h. Then the clusters relaxed and, within a few days, spontaneously dissociated into short, individual bar clusters. The short bar consisted of 3–5 primary globular particles in which size was as small as 30–50 nm. XRD showed that the particles were essentially a disordered nanocrystalline, which also displayed a slow relaxation behavior. We believe the synergistic interaction between polymer S630 and the surfactant docusate sodium played a key role in this drug suspension relaxation. Milling parameters such as time, speed, and stabilizer loading were altered to investigate their effects on relaxation.

Nanosized particles obtained through high-energy wet milling could be in a “far-from-equilibrium” state right after milling. The restricted diffusion and slow adsorption of stabilizer molecules leaves the surface of particles incompletely covered, which induce particles lined up to form a bar-like clusters, which may further bundle together and form a kind of ordering aggregation structure. Watershell particle morphology is highly asymmetric (i.e., bar, spindle configurations) and not dominated by Ostwald ripening. Gel formation in post-milling suspension system is a self-organization phenomenon in the non-equilibrium steady state. Over time, the suspension gradually separated into individual primary particles of a very small size. This process may be the result of acquiring repulsion through restricted adsorption of anion surfactant molecules Docusate sodium, which was trapped within narrow channel between particles. Upon achieving equilibrium, the particles should remain stable at a sub 100-nm level.

5. Conclusion

The nanoparticle suspension of Compound A was generated by formulating raw drug with special stabilizer combination and using high-energy wet milling. When milling stopped, nanoparticles agglomerated and the nanoparticle suspension formed large clumps or a gel within 1–2 days. The apparent size of the particles continued to increase until reaching a maximum size. Thereafter, the gel relaxed spontaneously with an apparent size reduction, and clusters automatically dissociated into individual particles of nano size within a few days. Following this, the suspension reached equilibrium and stayed at steady state. We studied this phenomenon by monitoring the particle size and morphology; the observed relaxation behavior following high-energy milling suggested the suspension was unstable and reorganization occurred far from thermodynamic equilibrium. Once the particle size decreased and big clusters dissociated into individual small particles, however, the system showed excellent long-term shelf stability. Ultimately, nanoparticle suspensions will be processed as dry powders for solid-dosage development,

and these forms must be re-dispersed into non-aggregated/non-agglomerated nanoparticulate suspension.

Our results suggest that milling conditions such as time, speed, and stabilizer concentration played an important role in the relaxation process that occurred in a nanoparticle dispersion. Altering these parameters resulted in an optimized milling process and improved product quality. Relaxation in nanosuspensions appears to relate to a non-equilibrium dissipative structure formed in a "far-from-equilibrium" state.

Acknowledgements

We would like to thank Dr. Yaodong Xu and Yongjin Yao for their valuable bioavailability measurements.

References

Bates, S., Zografi, G., Engers, D., Morris, K., Crowley, K., Newman, A., 2006. Analysis of amorphous and nanocrystalline solids from their X-ray diffraction patterns. Pharm. Res. 23, 2333–2349.

Chung, F.H., 1974. Quantitative interpretation of X-ray diffraction patterns. I. Matrix-flushing method of quantitative multicomponent analysis. J. Appl. Cryst. 7, 513–519.

Dressman, J.B., Amidon, G.L., Reppas, C., Shah, V.P., 1998. Dissolution testing as a prognostic tool for oral drug adsorption: immediate release dosage forms. Pharm. Res. 15, 11–22.

Food and Drug Administration, 2000. Guidance for Industry. Waiver of in vivo bioavailability and bioequivalence studies for immediate-release solid oral dosage forms based on a biopharmaceutics classification system. FDA, Rockville, MD, USA.

Kawashima, Y., 2001. Nanoparticulate systems for improved drug delivery. Adv. Drug Deliv. Rev. 47, 1–2.

Liversidge, G.G., Cundy, K.C., Bishop, J., Czekai, D., 1991, Surface modified drug nanoparticles, US Patent No. 5145684.

Merisko-Liversidge, E., Liversidge, G.G., Cooper, E.R., 2003. Nanosizing: a formulation approach for poorly-water-soluble compounds. Euro. J. Pharm. Sci. 18, 113–120.

Merisko-Liversidge, E., Sarpotdar, P., Bruno, J., Hajj, S., Wei, L., Peltier, N., Rake, J., Shaw, J.M., Pugh, S., Polin, L., Jones, J., Corbett, T., Cooper, E., Liversidge, G.G., 1996. Formation and antitumor activity evaluation of nanocrystalline suspension of poorly soluble anticancer drug. Pharm. Res. 13, 272–278.

Scherrer, P., 1918. Estimation of the size and internal structure of colloidal particles by means of Röntgen. Nachr. Ges. Wiss. Göttingen. 2, 96–100.

Shekunov, B., Chattopadhyay, P., Seitzinger, J., Huff, R., 2005. Nanoparticles of poorly water-soluble drug prepared by supercritical fluid extraction of emulsions. Pharm. Res. 23, 196–204.

Wissing, S.A., Muller, R.H., 2001. The influence of the crystallinity of lipid nanoparticle on their occlusion properties. Int. J. Pharm. 242, 377–379.